Electrical Properties of RF Sputtering Systems

A theory is developed that gives a relatively complete electrical characterization of rf sputtering systems. Three types of systems are analyzed: tuned substrate, driven substrate, and controlled area ratio of electrode (CARE) systems. The theory is applicable to any of these systems that do not use magnetic fields to confine the plasma. Given the input rf power and voltage at the target, and any other parameters that can be specified as independent variables (e.g., pressure, substrate drive voltage, tuning impedance, and system geometry), the theory provides explicit values for all dc and rf electrical parameters of the system. The dc bias developed at the substrate is explained and related to the resputtering energy. In addition, an approximate calculation is presented for the ion density in the plasma; this calculation allows a semiquantitative estimate of the rf voltage developed at the target for a given value of rf input power. It also shows the influence of pressure and frequency on rf sputtering system operation. Comparisons are made with real rf sputtering systems; these show that the theory is quite successful in predicting the operation of these systems. In addition, a much better understanding is achieved of some of the complex electrical phenomena encountered in these systems. The theory should prove useful both for new system design and for diagnostic work on existing equipment.

Introduction

In recent years a considerable body of experimental evidence has been accumulated indicating that in the rf sputtering of thin films, resputtering during deposition has an important influence on film properties [1-4]. Resputtering, presumably due to ion bombardment, is controlled primarily by the rf bias on the substrate holder; this was first shown by Logan[1] in his experiments with substrate tuning. From Logan's work it was apparent that similar results could be obtained by driving the substrate with an rf bias of known amplitude and phase.

While resputtering is strongly influenced by rf substrate bias, Koenig and Maissel [5] have demonstrated that resputtering may occur even when the substrate is grounded. Basically, a space-charge-limited sheath, describable at low pressures by the Child-Langmuir law, develops between the glow and all surfaces in the sputtering system. This sheath is capacitive, with the capacitance being dependent on the area, ion flux, and average potential across the sheath. The rf voltage applied to the target is divided between the capacitance of the target sheath and the capacitance of the ground sheath. Thus, an rf potential must exist between the highly conducting glow and

the grounded substrate. If that rf potential is sufficiently large—that is, if the ratio of the ground area to target area is sufficiently small, resputtering of the depositing film occurs.

This model, which is discussed more quantitatively in the paper by Koenig and Maissel [5], was also used by Logan [1] to explain his substrate tuning experiments. In those experiments, Logan found that when the impedance between substrate and ground was made increasingly inductive, a large negative dc potential developed on the substrate. However, when the inductance was increased beyond a certain critical value, the dc substrate potential changed discontinuously to a small, sometimes positive, value. This peak in negative dc substrate bias was attributed to resonance between the external inductance connecting substrate to ground and the capacitance of the sheath between substrate and glow.

The factors that control the bombardment of a growing film are thus explained qualitatively by two simple concepts. First, the sheaths present a highly capacitive impedance; second, the glow can be regarded as a highly conducting interconnection between these sheaths. The

Copyright 1979 by International Business Machines Corporation. Copyring is permitted without payment of royalty provided that (1) each reproduction is done without alteration and (2) the *Journal* reference and IBM copyright notice are included on the first page. The title and abstract may be used without further permission in computer-based and other information-service systems. Permission to *republish* other excerpts should be obtained from the Editor.

Figure 1 Equivalent circuit of an rf sputtering system.

purpose of this paper is to expand upon these concepts in order to obtain a quantitative understanding of the factors that control ion bombardment. The three techniques for controlling resputtering—tuned substrate, driven substrate, and controlled area ratio of electrodes (CARE)—are treated. The treatment goes beyond the calculation of ion bombardment; it yields a rather complete electrical

characterization of rf sputtering systems. This paper first presents a theory for rf sputtering system operation and then gives comparisons between the theory and available data. All notations used in the paper are listed in the Appendix.

Theory

Equivalent circuit of an rf sputtering system

A convenient starting point in the calculation of the electrical behavior of an rf sputtering system is the equivalent circuit shown in Fig. 1. This circuit is a slight generalization of the equivalent circuit given by Koenig and Maissel [5], and is also similar to that given by Logan [1]. The system comprises three electrodes: a target, a substrate holder, and the walls. The walls are defined to be the true rf and dc grounds. With the substrate drive voltage $V_{\rm d}$ equal to zero, the system is a tuned substrate system; with the impedance $Z_{\rm es}$ equal to zero, it is a driven system; with both equal to zero, it is a controlled area ratio electrode (CARE) system.

The circuits in Fig. 1 are numerically analyzed by standard techniques in the network analysis section of this paper, but before this can be accomplished, several other problems must first be addressed:

- 1. The relationship between the rf and dc voltages across the sheath at a boundary;
- 2. The relationship between the various dc sheath potentials and the externally measured dc substrate bias;
- 3. The dependence of sheath impedance on voltage and other variables; and
- 4. The factors controlling ion current density in the sheath and the factors controlling plasma resistance.

Relationship between rf and dc potentials across a sheath If the voltage across a sheath is of the form

$$V = V_{\rm dc} + V_0 \sin(\omega t), \tag{1}$$

and if the Maxwell-Boltzmann distribution holds for the electrons, the time average of the electron current density $\langle J \rangle_t$ through the sheath is [6]

$$\langle J \rangle_t = J_e I_o (e V_o / k T_e), \tag{2}$$

where J_e is the current density which would be drawn if $V_o = 0$,

$$J_{\rm e} = J_{\rm esat} \exp{(eV_{\rm dc}/kT_{\rm e})},$$

and I_o is the zeroth-order modified Bessel function of the first kind. If the sheath passes no net current, the average electron current density must be equal to the ion current density J_o [7]. Assuming that the ion current is independent of the sheath voltage (as expected for planar geome-

try) and that clipping of the sinusoidal voltage does not occur, the dc potential across the sheath is given by

$$\exp(-eV_{de}/kT_{e}) = J_{esat}I_{o}(eV_{o}/kT_{e})/J_{o}.$$
 (3)

When V_0 is zero, Eq. (3) reduces to the usual equation for the floating potential. Consequently, $\Delta V_{\rm dc}$, the change in dc potential due to the presence of the rf voltage, is given by

$$\exp\left(e\Delta V_{\rm dc}/kT_{\rm e}\right) = I_{\rm o}(eV_{\rm o}/kT_{\rm e}),\tag{4}$$

or

$$\Delta V_{dc}/V_{o} = (kT_{e}/eV_{o}) \ln \left[I_{o}(eV_{o}/kT_{e})\right]. \tag{5}$$

The total dc voltage across the sheath is the sum of $V_{\rm f}$, the floating potential in the absence of an rf voltage, and $\Delta V_{\rm dc}$. For $eV_{\rm o}/kT_{\rm e}$ much greater than one, Eq. (5) reduces to

$$\Delta V_{\rm dc}/V_{\rm o} = -1 + (kT_{\rm e}/2eV_{\rm o}) \ln (2\pi eV_{\rm o}/kT_{\rm e}).$$
 (6)

Equation 6 shows that for large values of $V_{\rm o}$ the negative bias developed across the sheath is approximately equal to the peak rf potential, as is known experimentally to be the case. Tsui [8] developed a similar result in a quite different calculation.

DC potentials in an rf sputtering system

In the previous section the dc potential across a sheath was related to the rf potential across that sheath by an equation of the form

$$V_{\rm dc} = -V_{\rm f} - V_{\rm o} \kappa(V_{\rm o}), \tag{7}$$

where $V_{\rm r}$ is the magnitude of the floating potential in the absence of any rf voltage and κ is a function of the peak amplitude of the rf potential $V_{\rm o}$. By applying this equation specifically to the wall sheath, $V_{\rm o}$ becomes $V_{\rm po}$, the peak rf potential of the plasma. The dc potential of the plasma relative to ground is then

$$V_{\text{pdc}} = V_{\text{po}} \kappa (V_{\text{po}}) + V_{\text{f}}. \tag{8}$$

Note that this potential is positive with respect to ground. Likewise, the dc potential between the plasma and the substrate is

$$V_{\text{psdc}} = -[V_{\text{pso}}\kappa(V_{\text{pso}}) + V_{\text{f}}]. \tag{9}$$

The negative sign indicates that the substrate charges negatively with respect to the plasma.

The measured dc substrate potential $V_{\rm sdc}$ is the sum of $V_{\rm pdc}$ and $V_{\rm psdc}$:

$$V_{\rm sdc} = V_{\rm po} \kappa (V_{\rm po}) - V_{\rm pso} \kappa (V_{\rm pso}). \tag{10}$$

If the rf voltages are large, κ is approximately unity, and

$$V_{\rm sdc} = V_{\rm po} - V_{\rm pso}$$
.

Thus, the measured dc substrate potential may be either positive or negative, depending on the rf potentials across the wall and substrate sheaths.

Sheath impedance

Koenig and Maissel, in their treatment of the low pressure rf sheath, assumed that the dc bias across the sheath determined the properties of the sheath. They used the Child-Langmuir law [9] to relate the sheath dimension (and consequently the sheath capacitance) to the dc voltage and the ion current density injected into the sheath. The relationship for the capacitance is

$$C = \zeta J_0^{1/2} A |\Delta V_{dc} + V_f|^{-3/4} ;$$

$$\zeta = 3/2 (M \epsilon_0^2 / 2e)^{1/4},$$
(11)

where A is the area of the sheath and $V_{\rm f}$ is the floating potential in the absence of an rf voltage, M/e is the mass-to-charge ratio of the ion, and $\epsilon_{\rm o}$ is the permittivity of free space. For argon, ζ has a value of 10^{-9} farad-volt^{3/4} per cm-amp^{1/2}.

Although Koenig and Maissel considered the sheath to be entirely capacitive, the equivalent parallel resistance can be defined in terms of the power dissipation in the sheath. Since the electrons drawn from the glow are never accelerated across a large potential difference, their power dissipation is negligible. The power dissipation is almost entirely due to the ion bombardment of the boundary and the consequent secondary-electron emission. The power dissipation associated with the rf voltage across the sheath is thus given [10] by

$$P = J_o(1 + \gamma)A|\Delta V_{dc}|, \tag{12}$$

where γ is the secondary-electron emission coefficient (second Townsend coefficient) and $\Delta V_{\rm dc}$ is the change in dc voltage induced by the rf voltage. The equivalent parallel resistance is

$$R = V_o^2 / 2P = V_o^2 / 2J_o(1 + \gamma)A |\Delta V_{dc}|.$$
 (13)

These equations are valid only at low pressures where the ions are not scattered as they traverse the sheath. At higher pressures, both scattering and ionization within the sheath tend to increase the space charge, and therefore the capacitance. Also, ionization causes an increase in the current through the sheath and consequently decreases the parallel resistance. The analysis of these effects is treated in a companion paper and the equations governing the sheath impedance are found there.

In the preceding sections it was assumed that the ion current density injected into the sheath was known; this is

not actually the case. The power dissipation is dominated by the target sheath because that sheath has by far the largest voltage across it. Consequently, if the power input and the voltage across the target sheath are known or can be calculated, Eq. (13) (or its more general equivalent in Ref. [11]) provides an approximate value for $J_{\rm o}$. However, this value is correct only in the vicinity of the target (or substrate, for usual geometries). It does not apply to the more diffuse glow that typically pervades the rest of the system.

The calculation of ion current densities is simplified by dividing the glow into two regions: an intense region in the vicinity of the target, and a more diffuse region pervading the rest of the system. This division is not arbitrary; it is based on empirical observation of the light generated by the rf discharge in typical sputtering systems.

We start with the assumption that the rate of creation of ions is proportional to the energy input to the glow. There are two contributions to the energy input and, thus, to the rate of creation of ions, $(dN_i/dt)_{\text{creation}}$. The two contributions result from a volume term due to scattering in the glow and a surface term due to secondary-electron emission from the boundaries,

$$(dN_{i}/dt)_{\text{creation}} = (\epsilon_{p}/E_{i}) \int_{v} \langle J_{\text{rf}} E_{\text{rf}} \rangle_{t} dv + \sum_{\text{sheaths}} (\epsilon_{s}/E_{i}) \gamma J_{o} V_{o} A, \qquad (14)$$

where the integrand is averaged over time. In this equation, $E_{\rm i}$ is the ionization energy, $J_{\rm rf}$ is the rf current density in the glow, $E_{\rm rf}$ is the rf field, v is the volume of the glow, γ is the secondary-electron emission coefficient, $J_{\rm o}$ is the ion current density in the sheath, $V_{\rm o}$ is the voltage across the sheath, and A is the area of the sheath. The values $\epsilon_{\rm p}$ and $\epsilon_{\rm s}$ are proportionality coefficients closely related to the first Townsend ionization coefficient [12], and give the fraction of total energy dissipated that produces ionization.

For equilibrium, the rate of creation is equal to the rate of loss of ions. Since recombination is negligible in argon at low pressure, the rate of loss of ions is given solely by the ion loss into the various sheaths. Thus,

$$(dN_{\rm i}/dt)_{\rm loss} = \sum_{\rm shorths} J_{\rm o} A/e. \tag{15}$$

We have assumed a system comprising two uniform regions. The following arguments suggest that we can assume negligible ion interchange between these two regions. The current density entering the typical target sheath must be of the order of 10⁻³ A/cm² if one is

to explain the observed sputtering rates. The ion current density calculated from the rate of injection from a Boltzmann distribution is far lower than this for reasonable ion densities and temperatures. It has been shown [13], however, that electron diffusion creates large fields at the edge of the glow, and these fields raise the ion energy to the order of $kT_{\rm e}$. Since the transition between high and low density regions is broad, the field at the transition is relatively weak. Consequently, any net particle interchange between the two regions should be small compared to particle loss to the sheaths.

With these assumptions we can write (for the targetsubstrate region)

$$(dN_{i}/dt)_{\text{creation}} = \epsilon_{p} I_{\text{rft}}^{2} f(D, A_{t})/2E_{i}e\mu_{e} n_{i}$$

$$+ \sum_{\text{sheaths}} (J_{o}/E_{i})\epsilon_{s} \gamma_{s} V_{s} A_{s};$$

$$(dN_{i}/dt)_{\text{loss}} = (J_{o}/e) \sum_{\text{sheaths}} A_{s}. \tag{16}$$

The function f, which depends on the distribution of rf current in the glow, is evaluated approximately in Appendix A; D is the target-substrate spacing, $I_{\rm rft}$ is the peak rf current flowing through the target, and here, $A_{\rm s}$ is the target area. The use of an electron mobility $\mu_{\rm e}$ is justified in argon if $E/p \gtrsim 0.015$ V/Pa-cm (>2 V/torr-cm). For argon [14],

$$\mu_{\rm e} = \frac{4.3 \times 10^7}{p} \text{ (Pa-cm}^2/\text{V-cm}; p \text{ in pascals)};$$

$$= \frac{3.2 \times 10^5}{p} \text{ (torr-cm}^2/\text{V-cm}; p \text{ in torr)}, \tag{17}$$

where p is the pressure. At low pressures, where Eq. (16) is valid, I_{rft} is given by [see Eq. (11)]

$$I_{\rm rft} = \omega V_{\rm to} C_{\rm t} = \omega \zeta J_{\rm o}^{1/2} A_{\rm t} V_{\rm to}^{1/4}. \tag{18}$$

When this equation is combined with Eq. (16), the result is

$$n_{\rm i} = \epsilon_{\rm p} \omega^2 \zeta^2 V_{\rm to}^{1/2} f(D, A_{\rm t}) A_{\rm t}^2$$

$$\div 2E_{\rm i} \mu_{\rm e} \sum_{\rm sheaths} [A_{\rm s} - (e \gamma_{\rm s} \epsilon_{\rm s} V_{\rm s} A_{\rm s} / E_{\rm i})]. \tag{19}$$

This relationship is quite useful from a conceptual standpoint because it shows that the low pressure rf discharge is not sustained by secondary electrons liberated from the target [15]. It is sustained instead by ionization in the glow due to the large rf currents flowing through the glow [16]. These large currents are possible only because of the capacitive coupling across the target sheath.

At low pressures, where secondary-electron effects can be neglected, Eq. (19) can be used to obtain the ion current density. Since the ion energy is of the order of $kT_{\rm e}$ when it enters the sheath [12], Eq. (19), evaluated explicitly for argon, reduces to

$$J_{o} = 1.5 \times 10^{-22} \epsilon_{p} \omega^{2} (kT_{e})^{1/2} V_{to}^{1/2} \left[\frac{A_{t}^{2}}{8D(A_{t} + A_{s} + A_{w})} \right]$$

$$(p \text{ in pascals})$$

$$= 2 \times 10^{-20} \epsilon_{p} \omega^{2} (kT_{e})^{1/2} V_{to}^{1/2} \left[\frac{A_{t}^{2}}{8D(A_{t} + A_{s} + A_{w})} \right]$$

$$(p \text{ in torr}). (20)$$

To obtain this result, the approximate treatment in Appendix A was used. The units for $J_{\rm o}$ in Eq. (20) are A/cm²; for $kT_{\rm e}$, eV; for ω , s⁻¹; for $V_{\rm t}$, volts; and for the dimensional factors, cm or cm². In Eq. (20) $A_{\rm w}$ is the wall area in contact with the intense glow. Equation (20) is useful for obtaining a rough estimate of the ion current density injected into the sheaths in the intense region. This equation is not, however, sufficiently accurate for use in the system analysis. Instead, a value of $J_{\rm o}$ is obtained that is consistent with the known rf power and voltage applied to the system.

The power dissipated in the glow can also be obtained from these equations. From Eqs. (14) and (15),

$$P_{\rm g} = \frac{J_{\rm o}E_{\rm i}}{e\epsilon_{\rm n}} \sum_{\rm sheaths} \left(A_{\rm s} - \frac{e\epsilon_{\rm s}\gamma_{\rm s}V_{\rm s}A_{\rm s}}{E_{\rm i}} \right). \tag{21}$$

Again, the terms in γ can usually be neglected at low pressures. It is fortunate that $P_{\rm g}$ is relatively small, for it is difficult to determine how this power dissipation should be incorporated into the equivalent circuit in Fig. 1. For the sake of simplicity we will attribute $P_{\rm g}$ entirely to a plasma resistance $R_{\rm pt}$ in series with the target. In this case,

$$R_{\rm pt} = 2P_{\rm g}/|I_{\rm rft}|^2,\tag{22}$$

and $R_{\rm ps}$, the plasma resistance associated with the substrate, is zero. This completes the analysis of the intense region.

The same arguments can be used to develop an expression for the ion density in the diffuse region. This analysis is contained in Appendix B. Only the results, as applied to argon, are given here. It should be noted that because secondary-electron effects are always negligible in the diffuse region, the validity of the results is not restricted to low pressures.

The scattering in the diffuse glow gives rise to a plasma resistance $R_{\rm pw}$ in series with the diffuse glow wall imped-

ance. From evaluation of Eq. (B4) in Appendix B,

$$R_{\rm pw} = 0.005 \ell_{\rm w} p E_{\rm os}^{1/2} / J_{\rm o}' A_{\rm w} \quad (p \text{ in pascals})$$

$$= 0.7 \ell_{\rm w} p E_{\rm os}^{1/2} / J_{\rm o}' A_{\rm w} \quad (p \text{ in torr}). \tag{23}$$

As noted earlier, $E_{\rm os}$, the energy with which the ion enters the sheath (in eV), is approximately equal to $kT_{\rm e}$. The ion current density into the diffuse region wall sheath, $J_{\rm o}'$, is given by

$$J_{o}' = 1.5 \times 10^{-22} \ell_{w} p \omega^{2} (\epsilon_{p} E_{os}^{1/2} V_{p}^{2} - 0.07 \ell_{w} p E_{os}) / V_{pwdc}^{3/2}$$

$$(p \text{ in pascals})$$

$$= 2 \times 10^{-20} \ell_{w} p \omega^{2} (\epsilon_{p} E_{os}^{1/2} V_{p}^{2} - 10 \ell_{w} p E_{os}) / V_{pwdc}^{3/2}$$

$$(p \text{ in torr}). \tag{24}$$

As explained in Appendix B, $\ell_{\rm w}$ is an effective length with a value of about 40 cm; $J_{\rm o}'$ is in A/cm², $E_{\rm os}$ in eV, and $V_{\rm p}$ and $V_{\rm pwdc}$ in volts. The term $V_{\rm pwdc}$ is the dc voltage across the sheath and is calculated from the rf voltage across the sheath $V_{\rm pw}$ by using Eq. (4); $V_{\rm pw}$ is calculated in turn from

$$V_{\rm nw} = V_{\rm p} |Z_{\rm w}/(R_{\rm nw} + Z_{\rm w})|, (25)$$

where the notation is explained in Fig. 1 and Appendix C. Equation (24) is used with Eq. (11) to calculate the capacitance of the sheath, and with Eq. (13) to calculate the parallel resistance of the sheath.

Because there is no explicit solution of these equations, numeric techniques must be used for the calculation. Note that J_o' is negative at very low values of V_p . This results from approximations in the derivation, and of course is not physically possible. Consequently, J_o' is assigned a zero value whenever V_p is low enough for Eq. (24) to give a negative result. This expresses the fact (experimentally observed) that when V_p is very small there is no ionization outside the intense region.

Network analysis

The analysis of the equivalent circuit in Fig. 1 can be made by using standard techniques. For the rf plasma voltage V_n ,

$$V_{\rm p} = \frac{Z_2 Z_3 V_{\rm et} + Z_1 Z_3 V_{\rm d}}{Z_1 Z_3 + Z_2 Z_3 + Z_1 Z_2},$$
 (26)

where Z_1 , Z_2 , and Z_3 are the impedances of the target, substrate, and wall branches of the network:

$$Z_{1} = Z_{et} + Z_{t} + R_{pt}, (27)$$

$$Z_2 = Z_{\rm es} + Z_{\rm s} + R_{\rm ns}, (28)$$

and

$$Z_3 = Z_w + R_{pw}. \tag{29}$$

The rf voltage across the substrate sheath is

7

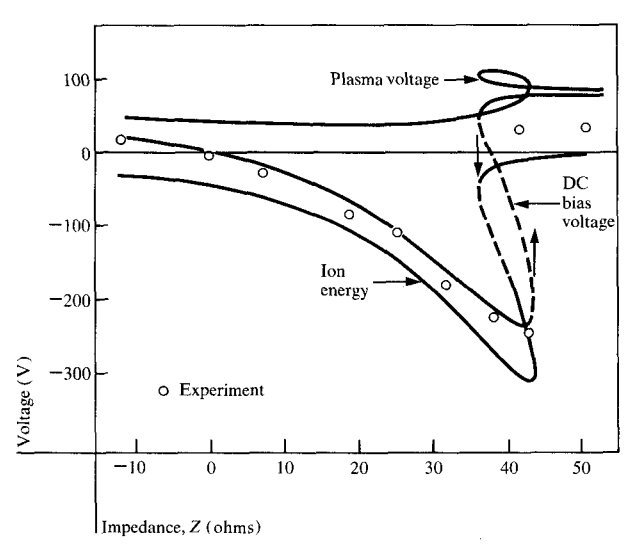


Figure 2 Calculated and measured dc voltages for a typical tuned substrate system.

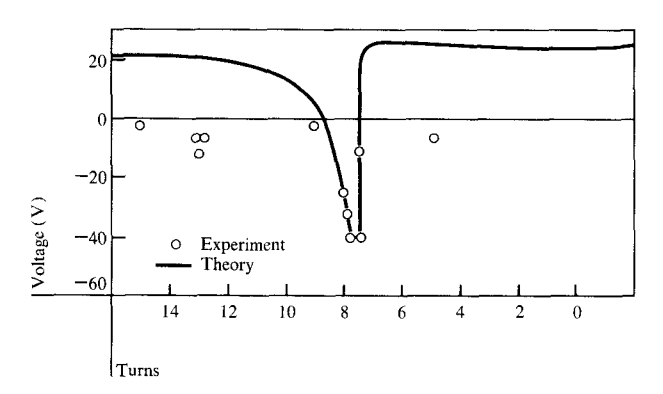


Figure 3 Calculated and measured dc substrate biases for a tuned substrate system with large wall area. The abscissa is proportional to the inductance of the series inductor in the tuning network. Note that the stray capacitance from substrate holder to ground must be accounted for in calculating the net impedance to ground.

$$V_{\rm ps} = V_{\rm p} - V_{\rm s} = (V_{\rm p} - V_{\rm d})(Z_{\rm s}/Z_{\rm 2}),$$
 (30)

across the target sheath it is

$$V_{\rm p} - V_{\rm t} = (V_{\rm p} - V_{\rm et})(Z_{\rm t}/Z_{\rm t}),$$
 (31)

and across the wall sheath it is

$$V_{\rm pw} = V_{\rm n}(Z_{\rm w}/Z_3 + R_{\rm pw}). \tag{32}$$

Each of these equations for a sheath voltage is expressed in terms of the plasma voltage and impedances, which are in turn functions of that particular sheath voltage. These sheath equations are also functions of the ion current density, the electron temperature (which fixes the floating potential), and other parameters that are specified at the start. The problem is thus reduced to finding values for the plasma voltage amplitude and phase that are consistent with the known target voltage and power, the substrate drive voltage and phase, or the substrate tuning impedance. Because of the highly nonlinear character of the sheath impedance, Eqs. (30), (31), and (32) for the three branches of the network must be solved by numeric techniques.

In most systems the intense region is in contact with the walls to some extent (usually the intense glow extends beyond the target rim for about 2 cm). Therefore, Eq. (29) was generalized to include a wall sheath impedance in parallel with the impedance of the diffuse region. This minor generalization does not change the character of the solutions, and does not affect the numeric techniques used in obtaining those solutions.

Numeric techniques for calculating system voltages

The details of the computer programming are too lengthy to be reported in this paper. It might be noted, however, that the programming was done in APL, an interactive terminal oriented language. The use of this language avoided much tedious automation of the iterative steps, because the operator could follow the key final iteration (where solutions are sometimes multiple-valued or non-existent) and interrupt the program when it was not converging.

A basic simplifying assumption was made in obtaining solutions to the various equations. A value of the ion current density in the intense region was obtained that was consistent with the known rf power and voltage applied to the target when the substrate was grounded [17]. This ion current density was held constant in all subsequent calculations of the effects of varying the substrate tuning impedance or drive voltage.

For the driven substrate case, Eqs. (14)-(25) were used as shown, with $Z_{\rm es}$ and $R_{\rm ps}$ defined to be zero. Once the value of ion current density was determined, a value for the plasma voltage amplitude and phase was found for each specified substrate drive voltage, amplitude, and phase that was consistent with the known target voltage.

A slightly different procedure was used to solve the equations for the tuned substrate system ($V_{\rm d}$ and $R_{\rm ps}$ defined to be zero). Again, $J_{\rm o}$ was determined from the values of rf input power and voltage for the grounded substrate condition. For that particular situation the rf input power is completely determined if either the plasma voltage amplitude or the amplitude of the voltage across the substrate sheath is given. Thus, the value of either of

these voltages that is consistent with the input power can be obtained by iteration. All iterations were carried out to an accuracy of one part in 10^6 .

Comparison of theoretical and experimental characteristics of rf sputtering systems

Three system types—tuned substrate, driven substrate, and CARE—are considered.

Tuned substrate systems

In the tuned substrate system a variable inductor and a blocking capacitor are placed in series between the substrate and ground. Typically, the substrate holder has a stray capacitance to ground of the order of 100 pF or more. The tuning network is usually designed to adjust over a range including both series resonance with the blocking capacitor and parallel resonance with the stray capacitance. If the inductor losses are reasonably small, this allows a wide range of reactance between substrate and ground [1].

Figure 2 shows the calculated and measured dc substrate biases for a system with a target area of 670 cm², a substrate area of 507 cm², and a wall area of 2400 cm². Of this wall area, 400 cm² was assumed to contact the intense region of the glow. A 20% power loss was assumed to occur in the impedance matching circuitry connected to the target input [18]. Other parameters required [1] were: $\omega/2\pi$ = 13.56 MHz, $\ell_{\rm w}$ = 40 cm (see Appendix B), $\gamma_{\rm t} = 0.2$, $V_{\rm f} = 15$ V, $\epsilon_{\rm p} = 0.4$ [12], stray capacitance in the substrate holder = 115 pF, and tuning circuit series resistance = 1.07 ohms. The value of γ_t was adjusted to give the correct reactance for the point of instability of the tuning curve; γ_t is probably too large, suggesting that power losses in the impedance matching circuit were greater than 20%. The calculated results are quite insensitive to the value of V_{ϵ} .

Figure 2 also shows the calculated dc voltages across the wall sheath $(V_{\rm pdc})$ and across the substrate sheath $(V_{\rm psdc})$. The sum of these two voltages is the measured dc substrate bias. The agreement between measured and calculated dc substrate biases is excellent, except for reactances beyond the instability, where the predicted bias is more positive than that measured. The voltage across the substrate sheath is a measure of the ion energies striking the substrate surface.

The peak in negative substrate bias has been attributed to series resonance between the inductive tuning network and the capacitive substrate sheath. However, if the losses in the substrate branch are not excessive, there are two other possible resonances: a series resonance with

the target sheath when the net impedance between plasma and ground is inductive, and a parallel resonance between the inductive substrate branch and the capacitive wall sheath. Each of these three resonances contributes to the electrical characteristics of the system. The series resonance with the substrate sheath causes a minimum in the plasma impedance and thus in the plasma voltage in Fig. 2. The series resonance with the target (a very low "Q" resonance) causes a slight dip in the rf input voltage near the point of instability. The parallel resonance between wall and substrate branches causes the maximum in the plasma voltage in Fig. 2. In order of increasing tuning reactance, these three resonances would occur as listed above. Because of the large wall capacitance, the resonances occur over a very small range of tuning reactance.

The instability, which occurs very near the parallel resonance condition, is caused by the voltage dependence of the sheath impedance. As long as the voltage across the substrate sheath increases when the tuning reactance is increased, the capacitance of the substrate sheath tends to decrease and the net change in reactance of the substrate branch is small. However, when an increase in tuning reactance causes the voltage across this sheath to decrease, the capacitance of the sheath increases and the net inductance of the substrate branch grows rapidly. This leads to the instability shown in Fig. 2.

Figure 3 shows the predicted and observed dc bias voltages for a tuned substrate system that has a much larger ratio of wall area to target area. This curve is for a 23-cm-diameter target in a metal chamber about 46 cm in diameter. Both the predicted and experimental curves show that the larger ratio of wall area to target area greatly reduces the maximum bias voltage that can be obtained.

The predicted curve for this system shows good agreement only in the region near the voltage peak. In measuring the bias voltage it is observed that the rf voltage on the substrate holder has harmonic content totaling almost 20 volts. This harmonic content may be partly responsible for the error between the predicted and observed bias voltages. One other factor which may affect the measured dc substrate bias is the presence of an insulating film on the substrate holder. Figure 4 shows a comparison between the observed and predicted bias voltages for the same system immediately after a 3.2-mm-thick molybdenum plate is placed on the substrate holder. Adding this plate apparently improves the dc contact to the substrate sheath, and may affect harmonic content as well. As is seen in Fig. 4, excellent agreement between theory and experiment is obtained over the whole region of the tuning curve.

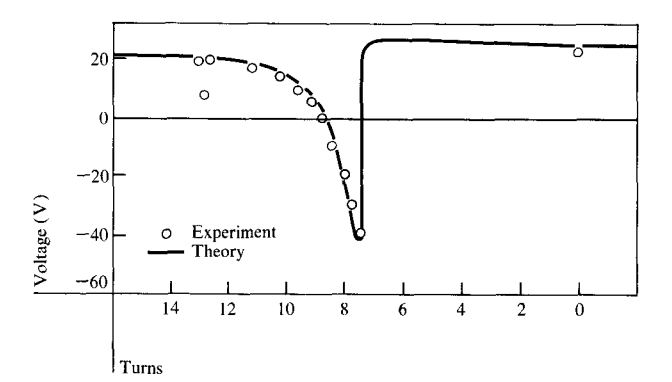


Figure 4 Calculated and measured dc substrate biases after the system characterized in Fig. 3 was modified to improve dc contact between the plasma and substrate holder.

Driven substrate systems

In a driven substrate system some of the rf power from the generator is used to drive the substrate holder at a given rf voltage and phase. Two synchronized generators may also be used for driving the target and substrate.

Figure 5 shows the predicted dc bias and ion bombardment voltage $V_{\rm ps}$ versus rf drive voltage for a given system geometry. The left-hand part of the plot corresponds to driving the substrate 180 degrees out of phase with respect to the target voltage; the right-hand part corresponds to driving it in phase. When the substrate is driven out of phase, the plasma voltage decreases and the bias and ion bombardment voltages increase fairly linearly with the rf drive voltage. The linear increase in dc substrate bias has been observed experimentally in several driven substrate systems.

The qualitative character of the substrate bias curve of Fig. 5 can be easily understood from Eq. (10), which shows that the net substrate bias is given approximately by the rf voltage across the wall sheath minus the rf voltage across the substrate sheath. Since the plasma voltage is nearly in phase with the target voltage when the substrate drive voltage is out of phase, the net rf voltage across the substrate sheath is the sum of the rf drive and plasma voltages. Thus, the substrate bias is

$$V_{\rm sdc} = V_{\rm po} - |V_{\rm d} + V_{\rm p}| \approx -|V_{\rm d}|.$$
 (33)

When the drive voltage is in phase, the voltage across the substrate sheath is the difference between substrate drive and plasma voltages,

$$V_{\rm sdc} = V_{\rm po} - |V_{\rm d} - V_{\rm p}| \approx 2V_{\rm p} - V_{\rm d} \quad \text{if } V_{\rm d} > V_{\rm p}.$$
 (34)

The decrease in plasma voltage as the out-of-phase substrate drive is increased may be qualitatively understood

from the fact that the rf plasma voltage is zero in a symmetric system when target and substrate voltages are equal. The substrate bias is zero for zero substrate drive because that corresponds to a grounded substrate.

An interesting glow intensification effect occurs with in-phase substrate drive. Since the system is basically a capacitive dividing network, the plasma voltage is nearly in phase with the target drive. Consequently, as the substrate drive is increased, the rf substrate current is first reduced and then reversed in sign. The net rf current through the wall sheath is thus increased as the in-phase substrate drive is increased, explaining the rise in plasma voltage. The increase in rf current to the walls also causes an increase in ionization in the glow; however, this phenomenon is not incorporated into these numeric solutions.

Changes in ion current density have little effect on the curves shown in Fig. 5, since those curves were generated assuming constant rf input voltage at the target. Just as in the CARE system model advanced by Koenig and Maissel [5], the ion current density terms in the sheath impedance cancel out in a calculation of the voltages across the sheaths. Indeed, with the assumptions in Ref. [5], Eq. (35) can be derived for substrate drive directly in phase (or, if the substrate drive voltage is negative, out of phase) with the target voltage:

$$V_{\rm p}^{1/4} = (V_{\rm t} - V_{\rm p})^{1/4} \frac{A_{\rm t}}{A_{\rm w}} \left[1 \pm \left(\frac{A_{\rm s}}{A_{\rm t}} \right) \left| \frac{V_{\rm d} - V_{\rm p}}{V_{\rm t} - V_{\rm p}} \right|^{1/4} \right], \quad (35)$$

where the positive sign holds when $V_{\rm d} > V_{\rm p}$, and the negative sign holds when $V_{\rm d} < V_{\rm p}$. The area ratio approximation derived in Ref. [5] is a special case of this equation.

Equation (35) supplies useful approximate values of the rf plasma voltage for given values of $V_{\rm t}$ and $V_{\rm d}$. However, the values predicted for $V_{\rm p}$ tend to be slightly low because of approximations made in the calculation of the sheath dimensions.

CARE systems

The area ratio approximation should be reasonably accurate for describing the operation of the CARE system at low pressures, if the system is designed to produce a large plasma voltage. Under these conditions, the real parts of the various impedances are small, and the capacitive divider model holds quite well. If the wall area is large, however, the plasma voltage is sufficiently small that approximations made in the calculation of the wall sheath impedance do not hold. In this case, deviations from the area ratio approximation can be substantial, as shown in Fig. 6. However, for most geometries and operating parameters, the error obtained by using the area ratio ap

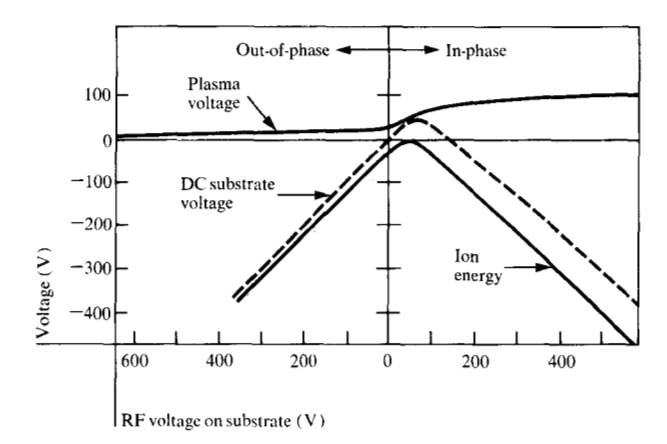


Figure 5 Calculated dc voltage for a system with the substrate driven either in phase or out of phase with the target.

proximation is little more than that likely to occur in estimating the floating potential $V_{\rm f}$. Consequently, the results obtained with the area ratio calculation are an excellent first approximation of the results obtained with these numeric calculations. The calculations in Fig. 6 were made assuming all of the system walls to be in contact with the intense region of the glow. This is a good approximation when the wall area is not too large.

At high pressures, scattering and ionization in the sheath decrease the distance across the sheath and increase the current density. These effects are much more pronounced in the higher-voltage sheaths. The high pressure CARE system is thus an interesting, if somewhat indirect, method for testing the pressure dependences of the sheath impedance equations.

In the high pressure CARE system the target dark space thickness is comparable to or smaller than the thickness of the usual 0.6-cm (0.25-in)-thick silica target. The voltage measured on the electrode in back of the target can therefore be much larger than the voltage across the target sheath. Figure 7 shows a comparison of the predicted and measured values of the voltage on the target surface, V_1 , as a function of pressure for a system run at constant rf power. The values of the rf input voltage, the dielectric target thickness, the rf power, and the pressure were used to calculate V_{i} ; the measured values were determined by a retarding potential technique [5]. The predicted values of V, are quite sensitive to the values of the Townsend coefficient and the secondary-electron coefficient. In this calculation a value of 0.1 ions/Pa-cm (14 ions/torr-cm) was used for the first Townsend coefficient, and 0.2 electrons/ion was used for the secondary-electron

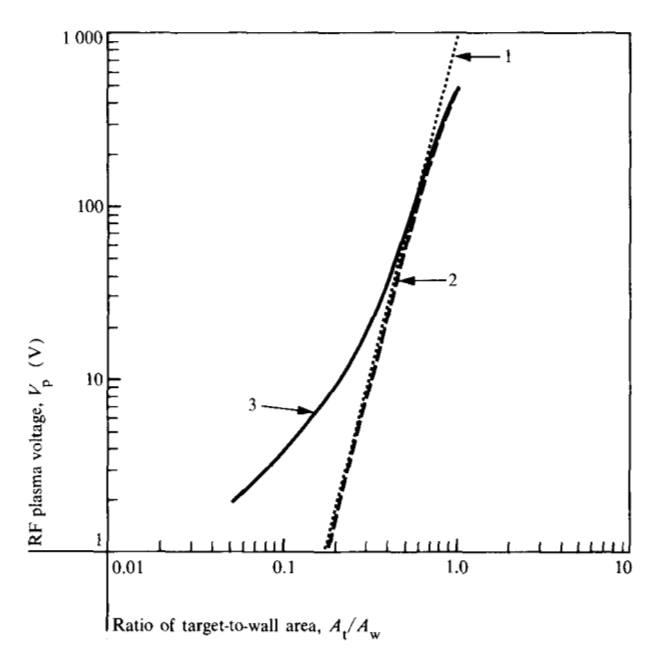


Figure 6 Calculation of a typical CARE system, showing the deviations from the area ratio approximation (curve 1) at low plasma voltages; $V_p = (A_t/A_w)^4 V_t$. When the area ratio is not small compared to unity, the area ratio approximation gives curve 2; $V_p = (A_t/A_w)^4/[1 + (A_t/A_w)^4]V_t$. Curve 3 represents the numeric analysis, assuming $V_t = 1000$ V, $p/A_t = 1$ W/cm², p = 1.3 Pa (0.01 torr), $\gamma_t = \gamma_w = 0.1$, and $V_t = 15$ V.

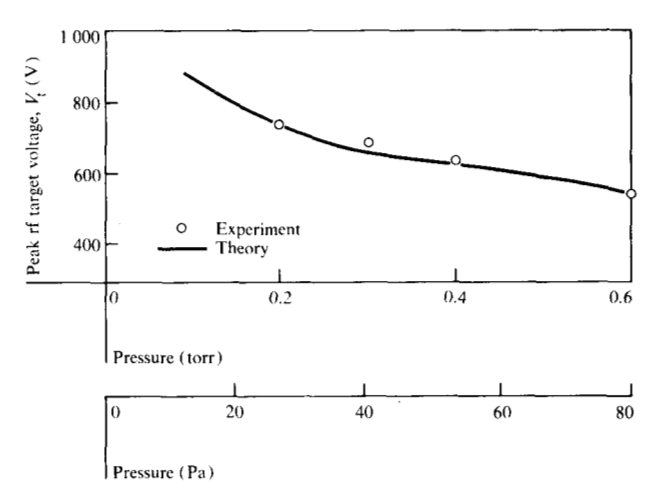


Figure 7 Calculated and measured rf voltages on the surface of the target (V_1) as a function of pressure in a CARE system.

emission coefficient. While 0.1 ions/Pa-cm (14 ions/torr-cm) may be a high value for argon [a better estimate is 0.08 ions/Pa-cm (11 ions/torr-cm)] [15], the need for this value may reflect some ionization by energetic neutrals in the dark space.

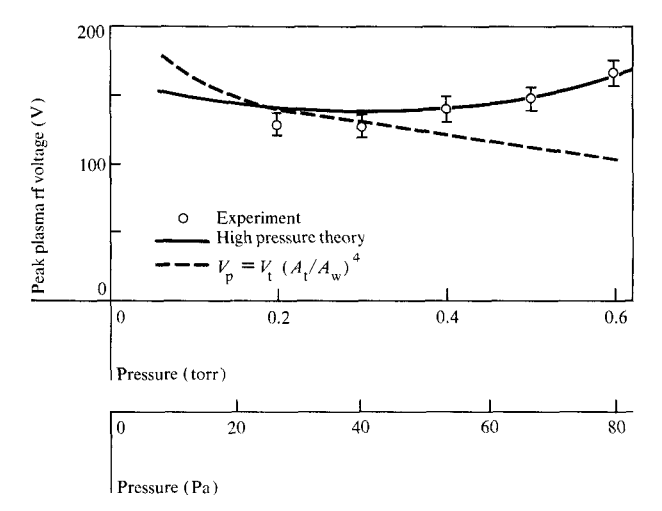


Figure 8 Calculated and measured rf plasma voltages as a function of pressure in a CARE system.

In a CARE system the plasma voltage corresponds to the ion bombardment potential at the substrate. Figure 8 shows a comparison between the predicted and experimental values of the plasma voltage vs pressure for a given area ratio. The experimental values were determined from curves of ion current vs retarding potential. If the area ratio approximation held, the plasma voltage would scale with the target potential, and would give the dashed line in Fig. 8. However, when the effects of pressure are included, the predicted plasma voltage increases with increasing pressure, in agreement with experiment. This increase in $V_{\rm p}$ is due to the reduction in target sheath impedance by scattering and ionization.

Conclusions

A model of electrical behavior has been developed that can be used for mathematical analysis of rf sputtering system operation. Calculated and measured electrical parameters are generally in good quantitative agreement for systems of widely varying geometry.

The most sensitive test of the model involves the calculation of tuning curves for the tuned substrate system. In this type of system the rf power and voltage applied to the target determine the ion current density in the sheaths of the intense region. The ion current density and the wall and substrate areas in turn determine both the reactance at which the tuning instability occurs and the dc substrate bias. The accurate prediction of the measured tuning curves is thus a very significant measure of the success of the model.

The only significant discrepancy between the calculated and measured tuning curves occurs at reactances

beyond the point of instability. In that region the theory predicts a positive substrate bias that is too large. This probably reflects the assumption that harmonics can be neglected. In this region of the tuning curve the amplitude of the fundamental rf signal across the substrate sheath is very small. Thus, if harmonics are present, their effects are most pronounced in this region. A similar problem exists in the calculation of the driven substrate curves—the predicted positive bias is again too large. Again, harmonic effects are probably responsible. Discrepancies can also be encountered if thick insulating films form on the substrate holder, such that contact between the substrate holder and the substrate sheath is affected.

The data taken with the high pressure CARE system appear to corroborate the sheath impedance equations. However, a somewhat high value of the first Townsend coefficient is required, possibly indicating ionization in the sheath by high energy neutral particles. It is unfortunate that no data are available on tuned substrate system operation at high pressures. As noted above, the tuned substrate system offers the most critical test of the model.

While the model is already capable of a number of quantitative predictions, it is still not in a form which allows complete *a priori* calculation of rf sputtering system operation. A few refinements are necessary before that becomes possible:

- Inclusion of magnetic field effects. These should be incorporated in terms of a magneto-plasma resistance. A magnetic field would not only increase the wall impedance, but might cause a variation in the resputtering rate across the substrate holder.
- 2. Refinement of the model for ion density in the intense region. The principal reason for this refinement is the prediction of glow intensification when the rf current through the substrate is small (or reversed, in the case of the driven substrate system). The model, at present, permits only a qualitative understanding of this phenomenon.
- Inclusion of harmonic effects. This is perhaps the most difficult refinement to make. Changes in harmonic effects are caused by seemingly minor variations in system design. Fortunately, the effect of harmonics typically appears to be small.

Perhaps the most fundamental assumption in this model is that the equivalent dc sheath can be used to calculate the rf impedance of a sheath. This particular aspect of the model is solidly verified. Another significant part of the model is the two-region approximation in analyzing the ion density in the glow. This part of the model appears to be verified by our ability to accurately calculate the

tuning curves using real system geometries. These tuning curves are moderately sensitive to the value of the wall area. Thus, if the two-region model were seriously in error, the tuning curves would not be correctly calculated.

In calculating the various curves, a number of parameters could only be estimated, for the most part from values given in the literature. One parameter which could only be guessed was the electron temperature $T_{\rm e}$ (which in turn specifies the floating potential $V_{\rm f}$ and the ion energy as it enters the sheath). Fortunately, the results of these calculations are virtually independent of the value of $T_{\rm e}$ for any reasonable choice of that parameter, unless the sheath voltages are very small.

Appendix A: Estimate of the function f

Equation (16), in the section on ion current density in the sheath, contains a function f which can be approximately evaluated.

We make the following assumptions:

- 1. The rf current flow through the substrate is negligible; the rf current therefore flows from the target to the walls.
- 2. The plasma voltage is sufficiently uniform that the rf current density in the target sheath is uniform.
- 3. The target and substrate are of equal area, and no walls contact the intense region.

Then the volume integral in Eq. (14) becomes

$$\frac{\epsilon_{\rm p}}{2n_{\rm i}e\mu_{\rm e}E_{\rm i}}\int_v |J_{\rm rf}|^2 dv,\tag{A1}$$

where $J_{\rm rf}$ is the peak rf current density in the intense glow.

For a cylindrical geometry, the integrated rf current density at a radius r from the target center is

$$J_{\rm rf} = \frac{I_{\rm rft}r}{2A.D}. (A2)$$

Substituting this in Eq. (A1) and integrating gives

$$f = 1/8D. (A3)$$

Appendix B: Calculation of the ion current density in the diffuse region

Starting with Eq. (14), and using the same reasoning that leads to Eq. (A1), one can write for the diffuse region

$$\left(\frac{dN_{i}}{dt}\right)_{\text{creation}} = \epsilon_{p} |I_{\text{rfw}}|^{2} \left(\frac{\ell_{w}}{A_{w}}\right) \frac{1}{e\mu_{e} N_{i}' e_{i}}, \tag{B1}$$

where I_{rtw} is the rf current to the walls of the system, N'_{i} is

the ion density at the edge of the wall sheath, and $\ell_{\rm w}$ is an effective length defined by

$$\frac{\ell_{\rm w}}{A_{\rm w}} \equiv \int_{\rm pe} \frac{|J_{\rm rf}|^2}{|I_{\rm pro}|^2} \frac{N_{\rm i}'}{N_{\rm i}} dv, \tag{B2}$$

where $v_{\rm d}$ represents the diffuse region volume, and $N_{\rm i}$ is the ion density at any given point in the diffuse region. This can be approximately evaluated as follows: Assume that the equipotential surfaces in the diffuse region have spherical symmetry, at least in the region where the integrand in Eq. (B2) is large. Let Ω be the solid angle defining the region where $J_{\rm rf}$ is large, and assume that $J_{\rm rf}$ is approximately constant for any radius r in that region. Finally, assume that the ion density varies as $1/r^n$. Then

$$\frac{\ell_{\mathrm{w}}}{A_{\mathrm{w}}} = \frac{1}{\Omega r_{2}^{n}} \int_{r_{1}}^{r_{2}} r^{(n-2)} dr.$$

Noting that the wall area $A_{\rm w}$ is given by $\Omega r_{\rm 2}^2$,

for
$$n = 0$$
, $\ell_{w} = \frac{r_{2}^{2}}{r_{1}} - r_{2}$;

for
$$n = 1$$
, $\ell_{w} = r_{2} \ln \left(\frac{r_{2}}{r_{1}} \right)$;

for
$$n > 2$$
, $\ell_{w} = \frac{r_{2}}{n-1} \left(1 - \frac{r_{1}^{n-1}}{r_{2}^{n-1}} \right)$.

A typical system might have a 50-cm diameter and a 15- to 30-cm-diameter intense glow region. (The intense glow extends visually a few centimeters beyond the edge of the target.) Thus,

for
$$n = 0$$
, $\ell_{yy} \approx 76-27$ cm;

for
$$n = 1$$
, $\ell_{yy} \approx 30-13$ cm;

for
$$n = 2$$
, $\ell_{w} \approx 18-10$ cm.

The diffuse glow is visually fairly uniform, corresponding to something between n=0 and n=1. Thus, the value for $\ell_{\rm w}$ is probably somewhere between 20 and 60 cm. In the third section, $\ell_{\rm w}=40$ cm was chosen as the best approximate value. If the system dimensions are substantially different from those used for this calculation, the value of $\ell_{\rm w}$ must be adjusted accordingly. Fortunately, the calculations are not very sensitive to the value of $\ell_{\rm w}$.

The rate of loss of ions from the diffuse region is given by

$$\left(\frac{dN_{\rm i}}{dt}\right)_{\rm loss} = \frac{J_{\rm o}'A_{\rm w}}{e},\tag{B3}$$

where J_0' is the ion current density injected into the wall sheath. Summing loss and creation rates, N_1' , the ion density at the edge of the wall sheath, is

$$N'_{i} = \frac{\epsilon_{p} |I_{\text{rfw}}^{2}| \ell_{w}}{\mu_{p} A_{w}^{2} J'_{0} E_{i}}.$$

In calculating $I_{\rm rfw}$, the plasma resistance must be included in the impedance. The plasma resistance $R_{\rm pw}$ is obtained by equating the power dissipation in the diffuse region, $R_{\rm pw}I_{\rm rfw}^2$, to the rate of loss of energy in the glow, as inferred from Eq. (B1). Then, noting that

$$N_{\rm i}' = \left(\frac{J_{\rm o}'}{e}\right) \frac{M}{2E_{\rm os}},$$

where J_0' is the ion current density in the wall sheath, M is the ion mass, and E_{os} is the ion energy as it enters the sheath, the plasma resistance is

$$R_{\rm pw} = \left(\frac{2}{M}\right)^{1/2} \frac{\ell_{\rm w} E_{\rm os}^{1/2}}{\mu_{\rm e} J_{\rm o}' A_{\rm w}} \ . \tag{B4}$$

It can be shown that whenever the real part of the wall impedance becomes comparable to the reactive part, the plasma resistance in turn is much larger than the real part of the wall impedance. Therefore, to a good approximation,

$$|I_{\text{rfw}}|^2 = \frac{V_{\text{p}}^2 \omega^2 C_{\text{w}}^2}{1 + \omega^2 R_{\text{pw}}^2 C_{\text{w}}^2},$$

where $C_{\rm w}$ is the capacitance of the wall sheath.

Combining these various equations then gives

$$J_{\rm o}' = \frac{\omega^2 \beta^2 g}{\kappa (V_{\rm pw} + V_f)^{3/2}},$$
 (B5)

where g is a function of V_{n} ;

$$g(V_{\rm p}) = \frac{e\epsilon_{\rm p}\ell_{\rm w}(2E_{\rm os}/M)^{1/2}V_{\rm p}^2}{2E_{\rm i}\mu_{\rm p}} - \frac{2\ell_{\rm w}^2E_{\rm os}}{M\mu_{\rm p}^2},$$
 (B6)

and recall that κ is a function of $V_{\rm pw}$. These equations, together with Eq. (B4), the circuit equations in the section on ion current density in the sheath, and the sheath impedance equations (7) and (9), can now be used to calculate the various parameters in the diffuse region.

Appendix C: Notations

$A_{\rm t}, A_{\rm s}, A_{\rm w}$	electrode areas of target, substrate, and walls
$C_{\rm t}, C_{\rm s}, C_{\rm w}$	sheath capacitances; subscripts as above
D	target-substrate spacing
$E_{ m i}$	ionization energy of gas
E_{os}	energy of ions as they enter a sheath
$rac{E_{ m os}}{E_{ m rf}}$	rf electric field in plasma or glow
e	electronic charge
f	a function evaluated in Appendix A
g	a function defined in Appendix B
$l_{\rm o}$	zeroth-order modified Bessel function of
	the first kind

$I_{ m rft}$	rf current flowing through the target electrode
$I_{ m rfw}$	rf current flowing to the grounded walls
$J_{ m esat}$	saturation electron current density
J_{o}, J_{o}'	ion current densities into sheaths in in-
	tense and diffuse glow regions
$J_{ m rf}$	rf current density in the intense glow
$J_{ m e}^{''}$	electron current density defined by Eq. (2)
$\langle j \rangle_t$	time average of electron current density
	through a sheath
k	Boltzmann's constant
$\ell_{\rm w}$	an effective system dimension evaluated
W	in Appendix B
M	ion mass
N_{i}, N'_{i}	ion density in intense and diffuse glow
	regions
P	rf power dissipated in the sheath
$P_{ m g}$	rf power dissipated in intense glow region
p	pressure
R	equivalent parallel resistance of sheath
$R_{\rm pt}, R_{\rm ps}, R_{\rm pw}$	plasma resistances associated with the
	target, substrate, and wall
$T_{ m e}$	electron temperature
t	time
V	voltage
$\Delta V_{ m dc}$	change in dc potential across a sheath due to the presence of an rf voltage
v	volume
$V_{ m f}$	floating potential in absence of rf across
¥7	the sheath
$V_{ m et}$	rf voltage applied to external target con-
	nection
$V_{\mathfrak{t}}$	rf voltage on surface of target
$V_{ m p}$	rf voltage at intense plasma region
$egin{aligned} V_{ m pw} \ V_{ m s} \end{aligned}$	rf voltage at edge of wall sheath
	rf voltage on surface of substrate
$V_{ m ps}$	rf voltage between plasma and substrate
	surface
$V_{\rm d}$	rf substrate drive voltage
	(If any of the above voltages occur with a
	subscript o (e.g., V_{po}), the quantity in-
	volved is the peak rf voltage. If the sub-
	script dc occurs, the quantity is the dc
	voltage at the given point.)
Z	impedance
$Z_{ m et}$	external impedance in target branch
Z_{es}	external impedance in substrate branch
$Z_{\rm t}$	target sheath impedance
$Z_{\rm s}$	substrate sheath impedance
$Z_{\mathrm{w}}^{'}$	wall sheath impedance
$Z_{1}^{"}, Z_{2}, Z_{3}$	see Eqs. (27), (28), and (29)
K	the ratio of $\Delta V_{ m dc}$ to the rf potential across
	the sheath. See section on dc potentials
	in an rf sputtering system.

a constant defined in Eq. (11) ζ second Townsend coefficient γ permittivity of free space fraction of electron energy producing ionization—p refers to the electrons in equilibrium in the plasma, s refers to the energetic secondary electrons emitted from the bombardment surfaces electron mobility $\mu_{\rm e}$ angular frequency of rf voltage (i)Ω solid angle defining the region where J_{rf} is

References and notes

- J. S. Logan, *IBM J. Res. Develop.* 14, 172 (1970); see also J. S. Logan, *Technical Report TR22.1653*, IBM System Products Division laboratory, East Fishkill, NY, 1973.
- L. I. Maissel, R. E. Jones, and C. L. Standley, *IBM J. Res. Develop.* 14, 176 (1970).
- 3. O. Christensen and P. Jensen, *J. Phys. E:* (Sci. Instrum.) 5, 86 (1972).
- 4. P. J. Burkhardt, L. V. Gregor, and R. F. Marvil, IBM Data Systems Division, E. Fishkill, NY; private communication.
- H. R. Koenig and L. I. Maissel, IBM J. Res. Develop. 14, 168 (1970).
- A. Garscadden and K. G. Emeleus, Proc. Phys. Soc. 79, 535 (1962).
- 7. We neglect secondary-electron emission from the boundary in this calculation.
- 8. R. T. C. Tsui, Phys. Rev. 168, 107 (1968).
- 9. K. T. Compton and P. M. Morse, Phys. Rev. 30, 305 (1927).
- 10. This result is correct when the ion energy distribution is symmetric about the energy in an equivalent strength. Tsui's calculation [8] suggests that this would be the case for all reasonable voltages in a sputtering system.

- 11. W. B. Pennebaker, *IBM J. Res. Develop.* 23, 16 (1979, this issue).
- 12. J. R. Acton and J. D. Swift, Cold Cathode Discharge Tubes, Academic Press, Inc., New York, 1963, p. 236.
- 13. J. E. Allen and P. C. Thonemann, *Proc. Phys. Soc. B* 67, 768 (1954).
- S. C. Brown, Basic Data of Plasma Physics, John Wiley & Sons, Inc., New York, 1959, p. 55.
- 15. According to Bleakney [Phys. Rev. 36, 1303 (1930)], a maximum of 11 ions/cm are produced in 133 Pa (1 torr) of argon by one electron. Therefore, at 0.13 Pa (10^{-3} torr), less than 0.055 ions can be produced by a secondary electron crossing a 5-cm glow. Since ϵ_1 is the fraction of energy dissipated in ionization by secondary electrons, the factor $e\epsilon_1 \gamma_1 V_1/E_1$ in Eq. (19) becomes 0.055 γ_1 . This is negligible for any reasonable value of γ_1 , particularly if the voltage V_0 on the opposing sheath is less than 50 V. See also E. W. McDanial, Collision Phenomena in Ionized Gases, John Wiley & Sons, Inc., New York, 1964, p. 189.
- 16. Another mechanism, "surf riding" of electrons on the oscillating edge of the sheath, appears to dominate at extremely low pressures.
- 17. The circuit equations simplify considerably when the substrate is grounded, making it easier to use iterative techniques in searching for the proper ion current density. More importantly, the solution for the plasma voltage is unique when the substrate is grounded.
- 18. Losses in the type of impedance matching circuit used are typically between 20 and 50%.

Received January 23, 1978; revised August 25, 1978

J. H. Keller is located at the IBM Data Systems Division laboratory, East Fishkill (Hopewell Junction), New York 12533; W. B. Pennebaker is located at the IBM Thomas J. Watson Research Center, Yorktown Heights, New York 10598.